analytical chemistry

ACS Editors' Choice

Article

pubs.acs.org/ac

Terms of Use

# Analysis of Protein Interactions with Picomolar Binding Affinity by Fluorescence-Detected Sedimentation Velocity

Huaying Zhao,[†] Mark L. Mayer,[‡] and Peter Schuck*[,†]

[†]Dynamics of Macromolecular Assembly Section, Laboratory of Cellular Imaging and Macromolecular Biophysics, National Institute of Biomedical Imaging and Bioengineering, National Institutes of Health, Bethesda, Maryland 20892, United States

[‡]Laboratory of Cellular and Molecular Neurophysiology, Porter Neuroscience Research Center, National Institute of Child Health and Human Development, National Institutes of Health, Bethesda, Maryland 20892, United States

Supporting Information

**ABSTRACT:** The study of high-affinity protein interactions with equilibrium dissociation constants ($K_D$) in the picomolar range is of significant interest in many fields, but the characterization of stoichiometry and free energy of such high-affinity binding can be far from trivial. Analytical ultracentrifugation has long been considered a gold standard in the study of protein interactions but is typically applied to systems with micromolar $K_D$. Here we present a new approach for the study of high-affinity interactions using fluorescence detected sedimentation velocity analytical ultracentrifugation (FDS-SV). Taking full advantage of the large data sets in FDS-SV by direct boundary modeling with sedimentation coefficient distributions $c(s)$, we demonstrate detection and hydrodynamic resolution of protein complexes at low picomolar concentrations. We show how this permits the characterization of the antibody−antigen interactions with low picomolar binding constants, 2 orders of magnitude lower than previously achieved. The strongly size-dependent separation and quantitation by concentration, size, and shape of free and complex species in free solution by FDS-SV has significant potential for studying high-affinity multistep and multicomponent protein assemblies.

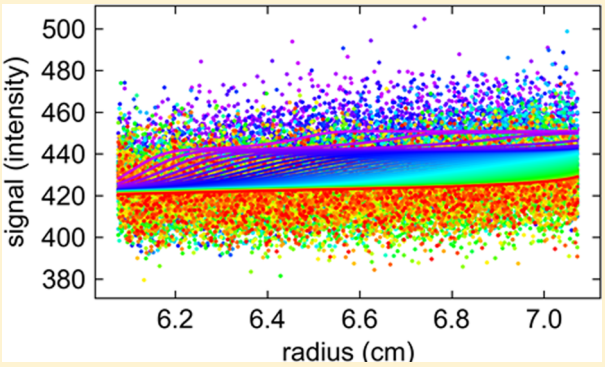


High affinity protein interactions are ubiquitous and play a central role in many spatiotemporal cellular structures, including, for example, regulatory multiprotein complexes, the quaternary architecture of ligand-gated ion channels, and immunological recognition processes.[1−4] Antibody−antigen interactions, in particular, are of key importance in biotechnology, for the development of potent protein pharmaceuticals and targeted drug delivery particles.[5−7] Thus, it is of substantial interest to accurately characterize basic thermodynamic parameters such as stoichiometry and free energy of binding, from which often further mechanistic insights can be derived, for example, on cooperativity and binding-induced conformational changes.[8] Even though some methods for the observation of high-affinity binding are widespread, for example, based on antibody capture in ELISA,[9] electrophoretic mobility shift assays for protein−DNA interactions,[10−12] and surface plasmon resonance (SPR) and other biosensors,[13,14] these may not be generally applicable to protein interactions, are not always sufficiently quantitative, and/or fail in the presence of more complex reaction schemes. On the other hand, classical methods of physical biochemistry for analyzing protein interactions are frequently very challenging to apply to high-affinity interactions, due to limited detection of the low concentrations required for the mass action law based equilibration short of saturation and/or due to the frequently slow equilibration.

In the present work, we describe a new addition to the toolbox for characterizing high-affinity binding in free solution, made possible by the previous introduction of a fluorescence detection system (FDS) as an accessory for the analytical ultracentrifuge (AUC).[15] By observing and modeling in detail the evolution of concentration profiles of dissolved macromolecules arising from the application of a strong centrifugal field, sedimentation velocity AUC is widely accepted as a gold standard for determining the number, size, and hydrodynamic shape of macromolecules and their complexes in free solution[16] and has emerged as a rigorous and popular tool for the study of reversible protein interactions.[17−19] Traditional applications of AUC are usually limited to the moderate and weak affinity range due to the limit of sensitivity of absorbance and Rayleigh interferometric optical detection systems.

The AUC fluorescence detection system has opened the possibility of significantly lower detection limits. Even though it was initially mostly thought of and used as a qualitative tool,[20−22] we have more recently developed data analysis

**Received:** January 8, 2014
**Accepted:** February 19, 2014
**Published:** February 19, 2014

   dx.doi.org/10.1021/ac500093m | *Anal. Chem.* 2014, 86, 3181−3187

models that account for the unique structure of FDS data, including optical effects of spatial gradients of signal magnification and temporal signal drifts arising from residual instability of laser power and potential photobleaching.[23] Jointly, with recent studies on AUC calibrations[24,25] and the choice of fluorescent labels in FDS,[26] this has unequivocally explained previously observed systematic deviations of FDS data from expected concentration profiles[22,27] and resolved discrepancies between sedimentation coefficients measured by conventional and FDS-detected AUC.[24,28] Thus, FDS-SV (fluorescence detected sedimentation velocity) has emerged as a highly quantitative method for detection of macromolecular sedimentation with a precision of the data and derived sedimentation parameters rivaling or even superior to conventional detection systems.[23]

In the present work, we develop experimental and analytical techniques for FDS-SV suitable for the detection of the sedimentation coefficient distribution of low picomolar protein concentrations and demonstrate how this method can be exploited to characterize the binding of enhanced green fluorescent protein (EGFP) to a bivalent monoclonal antibody with low pM $K_D$.

## EXPERIMENTAL SECTION

**Material.** Enhanced green fluorescent protein (EGFP) was prepared as described previously.[22,29] EGFP was dissolved in phosphate-buffered saline (PBS) containing 0.1 mg/mL carrier protein, unless noted otherwise. For carrier proteins, we tested bovine serum albumin (BSA), κ-casein, and lysozyme (A7030, C0406, and L6876, respectively, all acquired from Sigma-Aldrich, St. Louis, MO) and purified by size-exclusion chromatography. Monoclonal anti-GFP IgG D153-3 was purchased from MBL International (Woburn, MA).

**Sedimentation Velocity.** Sedimentation velocity (SV) experiments were carried out in an Optima XL-A analytical ultracentrifuge (Beckman Coulter, Indianapolis, IN) equipped with a fluorescence detection system (Aviv Biomedical, Inc., Lakewood, NJ) with a 10 mW laser emitting a wavelength of 488 nm. Fourteen samples at a range of concentrations were loaded in cell assemblies with standard 12 mm Epon double-sector centerpieces, installed in an 8-hole rotor, and placed into the rotor chamber for exhaustive temperature equilibration at 20 °C, typically for 2−3 h, followed by acceleration to 50000 rpm. The focal depth was set to 4 mm. For detection of the lowest concentrations, the photomultiplier voltage was set to ∼72%, gain was set to 8, and scanning angles, typically 1.0−1.2°, were adjusted to maximize exposure time individually for each sector without interference from autofluorescence of the Epon centerpieces. After ∼10−15 min, scanning was commenced at the highest possible rate for 12 h, with radial intervals of 20 μm.

**Data Analysis.** Sedimentation analyses were carried out in the software SEDFIT (version 14.3) and SEDPHAT (version 10.6), both available at sedfitsedphat.nibib.nih.gov. First, raw FDS data were sorted for analysis into lists containing ∼200−500 scans evenly spanning 40000 seconds of sedimentation time. These sets of fluorescence profiles were fit with sedimentation coefficient distributions $c(s)$.[30] Briefly, in this model a quasi-continuous distribution of theoretical sedimentation patterns of species with different $s$ values is fitted directly to the raw data, exploiting a hydrodynamic scaling law of compact particles to relate sedimentation and diffusion coefficient via a common, average frictional ratio. [30] The distribution was discretized with a grid of 100−150 $s$ values from 0 to 15 S, and maximum entropy regularization at a confidence level of $P = 0.68$ was used to produce the broadest distribution consistent with the data. In deviation from the standard protocol, [31] for data with low signal/noise ratios, no time- or radial-invariant baseline offsets and no FDS-specific refinements were used, the meniscus was determined graphically, and the average frictional ratio was fixed to the best-fit value from high signal samples. For binding analyses, $c(s)$ distributions were integrated from 1.0 to 9.5 S to create isotherms of fractional binding and signal weighted-average sedimentation coefficients ($s_w$) as a function of loading concentrations, and fit with mass action law models in SEDPHAT. Plots were created with GUSSI (http://biophysics.swmed.edu/MBR/software.html).

## RESULTS AND DISCUSSION

We have recently shown how the approach of direct global modeling of sedimentation boundaries with sedimentation coefficient distributions $c(s)$[30] can be extended to SV data with boundary signal amplitudes smaller than the statistical noise of the data acquisition,[22] due to the large number of data points ($10^4$−$10^5$) typically acquired over the time-course of a sedimentation experiment. For example, in an application to a study of the homodimerization of the AMPA receptor GluA2 ATD using absorbance optical SV, this permitted the determination of weighted-average sedimentation coefficients at protein concentrations as low as 11 nM.[22] We hypothesized that a similar approach would allow lowering the limit of FDS detection, which was previously reported to require 0.1 nM to 10 μM fluorescein for useful sedimentation analysis.[20,21]

To optimize the sensitivity of the detection, we significantly increased the FDS photomultiplier voltage above the level previously applied[22,23] and found an optimal signal/noise ratio at a setting of ∼72% for our instrument. Typical FDS-SV data at low picomolar concentrations of EGFP resemble those shown in Figure 1A. It is not obvious, and has not previously been explored, whether the stability and noise structure of FDS scans lend themselves for $c(s)$ analysis of low signal/noise data. However, even though it is difficult to visually discern the sedimentation process, the large number of scans and data points acquired leads to a well-defined peak in the $c(s)$ analysis, which is regularized with the maximum entropy method with uniform prior[32] so as to extract the least amount of information and broadest distribution consistent with the data (Figure 1B). The $c(s)$ peak is at an $s$ value of 2.59 S, highly consistent with previous results for monomeric EGFP at nanomolar to micromolar concentrations.[23] The calculated loading signal at 4 pM EGFP is 17.6 counts, slightly larger than the standard deviation of the statistical noise of data acquisition estimated to be 12.4 counts.

In the application of $c(s)$ to FDS-SV data with very low signal/noise ratio, we identified the following important points: an unavoidable correlation of the adjustable baseline offset with sedimentation patterns from species with extremely low sedimentation coefficients causes the maximum entropy regularization to generate a truncated peak at the low $s$ value end of the distribution (which is suppressed with Bayesian prior[33] only for the very first $s$ value). This can be diminished or sharpened by inclusion of scans from later times, which in the present case was taken up to at least twice the time required for the complete sedimentation of EGFP. Further, due to fewer informative scans reporting on species with higher $s$ values,


dx.doi.org/10.1021/ac500093m | Anal. Chem. 2014, 86, 3181−3187

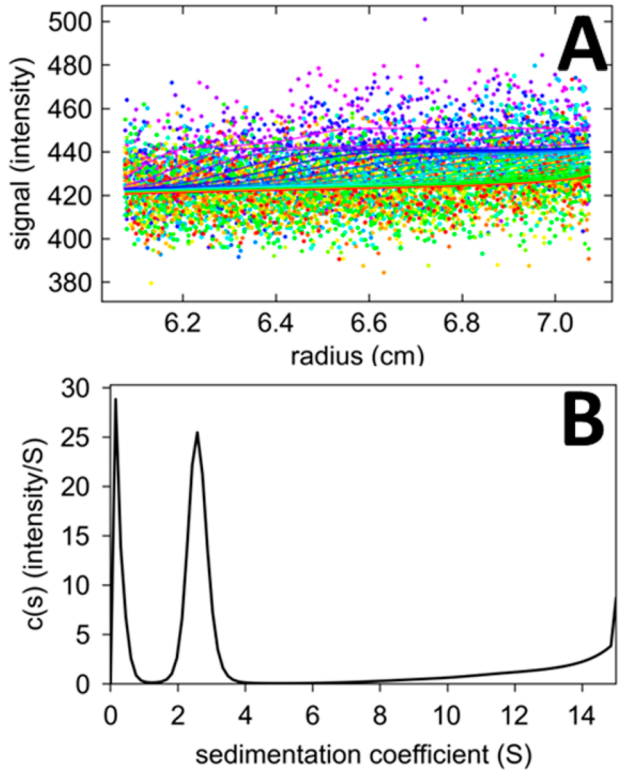


**Figure 1.** (A) Radial fluorescence scans of 4 pM EGFP at different times (dots) and best-fit boundaries from the $c(s)$ model (lines). For clarity, only every 2nd data point of every 20th scan is shown; higher color temperature indicates later times. Even though no migrating boundary pattern can be visually discerned in the noisy data, which is classically a prerequisite to sedimentation velocity analysis, this is not required in the modern analysis that is based on least-squares fits of explicit sedimentation models to the entire data set comprised of 247000 data points in 500 scans. (B) $c(s)$ distribution corresponding to the best-fit sedimentation boundaries in (A).

regularization may produce a shallow increase in $c(s)$ toward higher $s$ values; this could in theory be improved by faster data acquisition. This feature may also be contributed to by initial laser intensity drifts, and it is therefore important for the laser to be warmed up prior to data acquisition. Slight run-to-run variations in these factors and the absolute magnitude of noise can contribute variability of this feature. However, these features do not interfere with the integration and further analysis of the clearly developed main peak.

The meniscus position is an essential parameter for the accurate determination of sedimentation coefficients. In standard FDS-SV, there is no fluorescence signal associated with the meniscus; it cannot be recognized from characteristic optical artifacts at the air/water interface as in conventional AUC with absorbance or Rayleigh interference optical detection. Furthermore, at low signal levels it cannot be implicitly defined as an adjustable parameter in the sedimentation boundary analysis. To address this problem, Bailey et al.[34] have previously proposed creating an artificial interface with a layer of floating oil spiked with a fluorophore. However, this procedure turned out to be unnecessary: at the high PMT voltage used in the present study, we invariably observed a baseline signal shift by ~40 counts at the radius of the transition from air to the aqueous solution column (Figure S1A of the Supporting Information). We believe this to arise from Raman scattering of water: Our FDS instrument has a fixed excitation at 488 nm and a fixed bandpass for detection from 505 to 565 nm, which partially overlaps with the Raman shifted emission of water at low wavenumbers. Even though the commercial detection system does not currently provide wavelength resolution to measure the emission spectrum, the notion that the signal increase at the air/water interface is due to Raman scattering is supported by the observation of significantly stronger signals for water/ethanol mixtures, as well as for pure $D_2O$, as would be expected from the lower frequency of C−H and O−D stretching as compared to O−H[35,36] (Figure S1, panels B and C, of the Supporting Information). Therefore, the water Raman signal unexpectedly offers a convenient marker for the graphical definition of the meniscus, eliminating potential concerns of fluorophore or protein adsorption or degradation at an artificial water/oil interface. With the width of the signal of the air-to-water interface being ~0.015 cm, the associated errors in $s$ values are ~ ±1%.

To prevent loss of protein by adsorption on the surface of cell assembly components, the addition of an inert carrier protein is indispensable when working at subnanomolar concentrations.[20] Following common practice,[20,22,37,38] initially we used BSA at 0.1−0.5 mg/mL for this purpose but observed significant signal contributions scaling in amplitude with BSA concentration (Figure S2 of the Supporting Information). For example, at 0.5 nM EGFP in the presence of 0.5 mg/mL BSA, a trace of 2.8% of the total signal could be resolved sedimenting at 4.3 S, which corresponds to the characteristic $s$ value of BSA monomers. The relative contribution of the BSA signal increased with decreasing EGFP concentration, such that at 4 pM EGFP, the BSA monomer peak and a smaller dimer peak constitute the dominant signals even at the lowest suitable BSA concentration (0.1 mg/mL) (Figure S2 of the Supporting Information). Such signals may arise from scattering and imperfections in the emission filters, from Raman scattering, and/or as a result of fluorescent ligands bound to BSA;[39,40] notably, however, they could not be removed by size exclusion chromatography or exhaustive dialysis (data not shown). Although a separate measurement of the carrier protein allows one to account for these signal contributions to the weighted-average $s_w$ value of the fluorescent protein of interest and its complexes, and the BSA contributions may in favorable cases be hydrodynamically resolved (Figure S2 of the Supporting Information), a preferable approach is the use of a carrier protein that does not show significant fluorescent signal contributions. This was the case for ~0.1 mg/mL lysozyme or 0.075−0.2 mg/mL κ-casein, both chromatographically purified. The latter was used in the following experiments.

A second critical aspect for the choice of carrier protein is that it be inert toward the protein(s) of interest. This can be tested by FDS-SV or conventionally detected SV at higher protein concentrations in the presence and absence of carrier. For any given protein, this needs to be tested. For example, the use of κ-casein may potentially be problematic, considering the associated phosphate groups, lysozyme considering its positive charge (pI 11.4), and BSA considering its propensity for binding a large number of compounds. The relative size of the carrier to the protein of interest did not appear to play a significant role, as 0.1 mg/mL aldolase (MW 157 kDa) functioned as an efficient carrier for EGFP despite its much faster sedimentation.

Sedimentation coefficient distributions of EGFP at low picomolar concentrations are shown in Figure 2. Below 1 pM,


dx.doi.org/10.1021/ac500093m | Anal. Chem. 2014, 86, 3181−3187

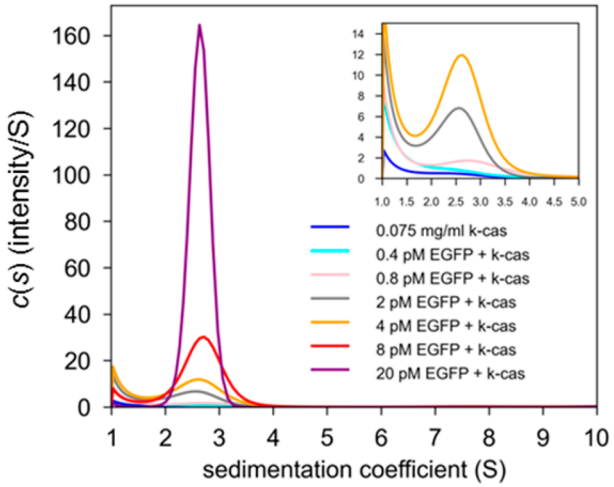


**Figure 2.** Sedimentation coefficient distributions of EGFP at various concentrations in PBS with 0.075 mg/mL $\kappa$-casein.

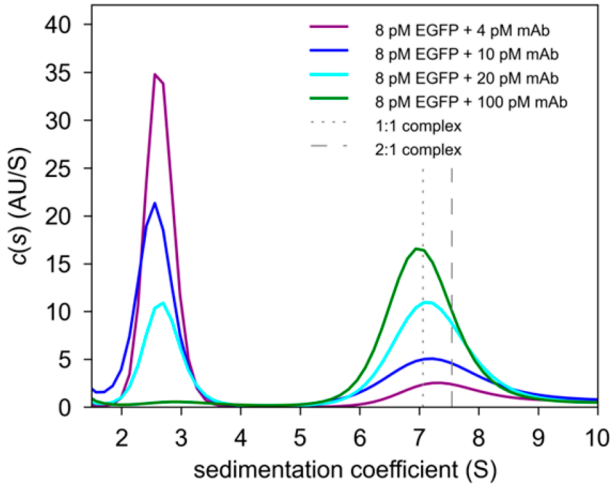


**Figure 3.** Titration series of 8 pM EGFP with mAb in PBS with 0.1 mg/mL $\kappa$-casein. *s*-values of 1:1 and 2:1 complexes were determined from experiments under stoichiometric conditions with EGFP or mAb in excess, respectively.

no reliable signal was obtained. However, >1 pM could be reproducibly detected and at >2 pM EGFP, the reliable quantitation of the sedimentation coefficient distribution is possible.

In order to test if this high sensitivity of detection can be utilized to characterize protein interactions at picomolar concentrations, we chose the system of EGFP, interacting with a monoclonal anti-GFP antibody (mAb). The same antibody−antigen system was previously chosen by Kroe & Laue[20] as a model for demonstrating the capabilities of the FDS, but no $K_D$ could be determined by FDS in the previous study and, unexpectedly, the presence of only 1:1 complexes was reported. In light of the well-known bivalency of IgG antibodies,[41] the authors hypothesized steric hindrance to occur, even though structural considerations would make this rather unlikely.[41] Thus, we anticipated that revisiting this system would highlight whether these molecules interact in an unusual mode or whether there are intrinsic problems with FDS-SV, yielding incorrect stoichiometries.

With the approach described above, we were able to conduct mixing experiments of EGFP and mAb at up to 20000-fold lower EGFP concentrations than studied previously.[20] As shown in Figure 3, significant binding is apparent from the detection of faster sedimenting components at ∼7−8 S at pM concentrations of EGFP. We believe that detection of a single complex peak has previously led to misinterpretation of the stoichiometry of the EGFP-mAb complex formation.[20] However, due to the relatively small mass difference of EGFP and IgG, 1:1 and 2:1 complexes (∼180 kD and 210 kD, respectively), resolution of these species as two peaks would not be expected. Nevertheless, the data in Figure 3 show a peak shift, from 7.12 S at 8 pM EGFP and 100 pM mAb to 7.35 S at 8 pM EGFP and 4 pM mAb, reflecting different majority populations of single and double occupied complexes when conditions with excess EGFP are compared with those of excess mAb, consistent with the expected bivalency of the IgG antibody. Similar peak shifts are observed in all titration series at constant EGFP at higher concentrations (data not shown). Finally, in experiments at high concentrations leading to essentially stoichiometric binding, conditions with greater than 2-fold excess of EGFP over mAb led to a complex *s* value of 7.55 S, whereas with 2.1-fold excess of mAb over EGFP, an average complex *s* value of 7.18 S was observed (data not shown). This led to an s value of 7.06 S for the 1:1 complex after accounting for binominal statistics of single- and double-occupied complexes and corroborating the formation of both 1:1 and 2:1 complexes, as expected on the basis of the IgG structure.[41]

For quantitative analysis of binding affinity, experiments at various concentrations of EGFP and mAb were carried out. The total EGFP signal was found to be independent of mAb concentration, showing the absence of quenching in the complex, and, trivially, there was no signal contribution of the free antibody. From the calculated $c(s)$ traces of each experiment, different binding isotherms are available: (1) The overall signal average sedimentation coefficient, $s_w$, from integration of both free and complex peaks of $c(s)$, follows the corresponding signal average *s* value of species populations predicted from mass action law, irrespective of the reaction kinetics.[42] It is intimately related to the overall mass balance (corresponding to the change in area under the boundaries) and, therefore, can be reliably determined without hydrodynamic resolution of different species.[42,43] (2) The fraction of signal sedimenting in the complex relative to the total signal as a function of antibody concentration and (3) the average *s*-value of the complex peak (experimentally least well-determined at very low levels of complex) can be modeled either with mass action law for reactions with complex lifetimes that are slow on the timescale of sedimentation or with the effective sedimenting particle model[44] for reactions that are fast on the timescale of sedimentation.

Taking advantage of the large number of samples that can be run in a single experiment with FDS, a global analysis was performed for a series of 14 samples with different concentrations and molar ratios of EGFP and mAb. For the analysis, we implemented a model in SEDPHAT, based on the mass action law with two equivalent sites and mixed EGFP:mAb complexes of 1:1 and 2:1 stoichiometry, that fits the isotherms of free and total bound EGFP signal (which is the sum of both complexes) and does not require the distinction in the experimental data between the different stoichiometry complexes. This led to best-fit values for the microscopic $K_D$ of the equivalent sites of 20.5 pM (95% CI 16.9−25.4) and sedimentation coefficient of 7.19 S (95% CI 6.96−7.43) and


dx.doi.org/10.1021/ac500093m | *Anal. Chem.* 2014, 86, 3181−3187

8.02 S (95% CI 6.87−9.12) for the 1:1 and 2:1 complex, respectively (Figure 4). (When both complex $s$ values were

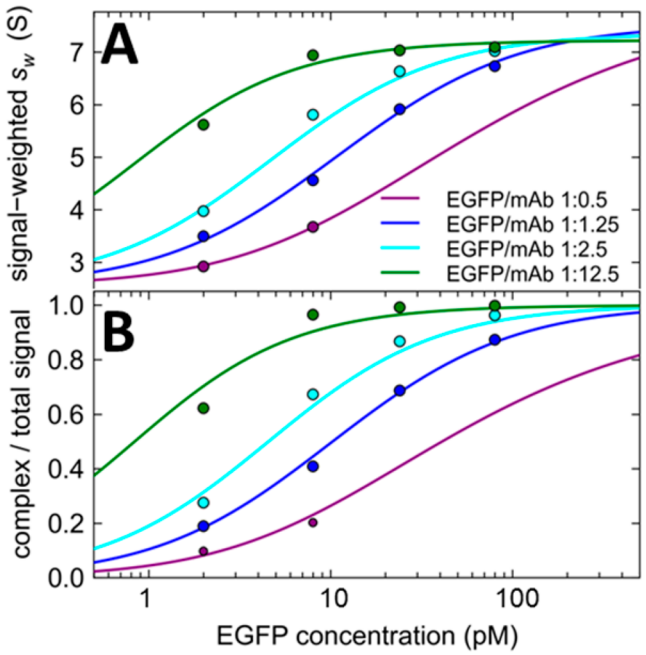


**Figure 4.** Measured binding isotherms (symbols) of (A) signal-average sedimentation coefficients ($s_w$) as a function of composition for different titration series of fixed EGFP and variable mAb concentration and (B) the signal fraction of bound EGFP for the same experiments. A global analysis of all data shown with a model of each mAb having two equivalent sites for EGFP results in best-fit isotherms (lines) with $K_D$ = 20.5 pM.

constrained to the values estimated for the complexes under conditions of essentially stoichiometric binding, as described above, a best-fit microscopic $K_D$ of 18.1 pM was determined at a slightly narrower 95% CI of 16.0−21.4 pM.) This corresponds to values for the macroscopic binding constants of ∼10 and ∼40 pM, respectively.

A crucial question when carrying out binding experiments for high-affinity interactions is whether the reaction has come to thermodynamic equilibrium. This may not be a priori obvious, as high-affinity systems, in particular, may exhibit very slow chemical off-rate constants. To examine the potential influence of sample equilibration kinetics, we performed kinetic simulations (Methods S1 of the Supporting Information). Our results suggest that if the measured bound fractions are kinetically limited, they will still monotonically increase with concentration and may even be satisfactorily fitted with impostor equilibrium binding models where the isotherm midpoint is shifted to higher concentrations (Figures S3 and S4 of the Supporting Information). Kinetic simulations suggest that nonequilibrium experiments impose a limiting apparent affinity on the order of $K_{D,app} \geq (t_{exp} \times k_{on})^{-1}$ (where $t_{exp}$ is the incubation time and $k_{on}$ is the chemical on-rate constant) irrespective of the true $K_D$, which may be much lower. Antibody−antigen reactions, typically have on-rate constants $k_{on}$ in the range of $10^6$−$10^8$ $M^{-1}$ $sec^{-1}$.[45] For example, if an interaction with a true $K_D$ of 10 pM and $k_{on}$ of $10^7$ $M^{-1}$ $sec^{-1}$ ($k_{off}$ = $10^{-4}$ $s^{-1}$) was allowed to incubate for only 100 s, the resulting binding isotherm would be well-described with an apparent $K_{D,app}$, an order of magnitude above the true value (or 2 orders of magnitude above the true value for $k_{on}$ = $10^6$ $M^{-1}$ $sec^{-1}$ and $k_{off}$ = $10^{-5}$ $s^{-1}$, respectively). On the other hand, with incubation times of 10000 s, which is comparable with the experimental timescale of SV, the overestimate of $K_{D,app}$ would amount to only 10% (or a factor of 2, respectively). Thus, the slow timescale of SV with equilibration times on the order of a few hours appears to be a virtue, rather than limitation.

Kinetically limited binding assays may be readily identified by increasing the incubation time (leading to a proportionally lower $K_{D,app}$) and/or by carrying out side-by-side experiments directly mixing the reactants in combination with dilutions of pre-equilibrated stock mixtures that are allowed to relax for different lengths of time, as shown by simulations in Figures S5 and S6 of the Supporting Information. Thus, we tested our FDS-SV study of the EGFP and mAb for kinetic control with pre-equilibration/dilution experiments. A mixture of 40 pM EGFP and 100 pM mAb was prepared by mixing aliquots from stock solutions of each protein. From this sample, after incubation for a time $t_{100pM}$, we took aliquots, diluted them 10-fold to a final concentration of 4 pM EGFP and 10 pM mAb, and let them relax to the new equilibrium for different times $t_{10pM}$ prior to SV. With $t_{100pM}$ of 1020 s and $t_{10pM}$ of 18600 s, we measured an $s_w$value of 4.89 S; with $t_{100pM}$ of 16020 s and $t_{10pM}$ of 4600 s, we measured 4.85 S. (As a control, the original sample of 40 pM EGFP + 100 pM mAb with $t_{100pM}$ of 19600 s without dilution yielded an $s_w$ value of 6.49 S.) Finally, a sample of 4 pM EGFP + 10 pM mAb was prepared by directly mixing aliquots from separate stock solutions of each protein, and incubated for only 4600 s prior to SV, leading to an $s_w$ value of 4.75 S. The $s_w$ values of the different 4 pM EGFP mixtures are very close and consistent within error, which demonstrates that all mixtures are close to equilibrium, irrespective of whether attained through predominantly assembly or dissociation processes. Therefore, for this high-affinity protein binding system, the slow kinetics of the dissociation of the complex does not seem to have significant impact on the FDS-SV results.

It is of interest to compare FDS-SV with other biophysical techniques for determining the binding properties. Optical biosensing (such as SPR) is an attractive approach for its direct observation of the binding kinetics. However, for reliable measurements of $K_D$, it still requires experimental times on the order of $1/k_{off}$. A particular concern for interactions with picomolar affinities is that at high on-rate constants, diffusional transport to the surface becomes limiting, whereas for low offrate constants, the baseline stability of the instrument limits accurate measurement of slow dissociation kinetics.[14]

We conducted an SPR biosensor experiment with immobilized mAb flowing EGFP across the sensor surface (Figure S7 of the Supporting Information). As is typically the case in SPR, the measured sensorgrams showed strong deviations from the expected pseudo-first-order binding progress.[14,46] However, a model accounting for a continuous distribution of affinity and rate constants[46] described the data well, reflecting significant heterogeneity of sites induced by immobilization and/or heterogeneity of the physical and chemical microenvironment of the sensor surface and polymeric immobilization layer. The largest population (comprising 48.8% of sites) was found to be at $K_D$ ∼ 0.16 nM and $k_{off}$ ∼ 3 × $10^{-4}$ $s^{-1}$. This is 8-fold weaker than observed by FDS-SV, highlighting commonly observed (but protein dependent) discrepancies of affinities for surface-immobilized molecules versus solution affinities.[14,47,48] In principle, an SPR competition approach could be used to


dx.doi.org/10.1021/ac500093m | Anal. Chem. 2014, 86, 3181−3187

determine the solution $K_D$;[14,47−49] however, this may not be practically applicable for systems with $K_D$ < 0.1 nM.[49] In the present case, it was precluded due to the unexpected cross-reactivity of soluble mAb to the sensor surface (which may account for the lower affinity of immobilized mAb for free EGFP; data not shown). This highlights the advantageous capability of FDS-SV to allow the observation of binding in free solution, in the absence of any matrix, filter, or other surface. Even though fluorescent labeling will generally be required, which itself carries the potential for artifacts,[26,50] it is often possible to use competition experiments between labeled and unlabeled proteins to determine the $K_D$ for the interaction between unlabeled molecules,[21] similar to the surface competition approach in SPR.

Another approach for measuring high-affinity interactions that combines fluorescence detection with hydrodynamic separation of free and complex species has recently been described on the basis of size-exclusion chromatography.[51] While it is even more sensitive with femtomolar detection limits, we believe FDS-SV, where applicable, will offer several advantages: first, the hydrodynamic resolution in SV is generally stronger (if $R_S$ is the particle Stokes radius, the resolution in SV is dependent on $R_S^2$, but in size-exclusion chromatography it is dependent on $R_S^{-1}$), and separation is quantitative. Second, rigorous frameworks for data analysis are available in SV independent of the reaction kinetics,[42,44,52] whereas chromatographic separation requires slow dissociation. Finally, some proteins interact with the matrix during size exclusion chromatography, while SV experiments are performed in free solution in a matrix free environment.

Other spectroscopic methods such as fluorescence anisotropy and fluorescence cross-correlation spectroscopy in a standard gravitational field are usually not sufficiently sensitive for determination of $K_D$ below 0.1 nM.[53−56] Like fluorescence spectroscopy and energy transfer methods, they usually do not lend themselves equally well as SV to determine the number and size of complexes formed,[57] although these techniques share other advantages, such as compatibility with microscopy and in vivo applications. Another popular method for studying protein interactions, isothermal titration calorimetry (ITC), lacks the sensitivity for the measurement of sub-nanomolar $K_D$'s and leads to stoichiometric binding at cell concentrations with detectable enthalpies (high "$c$ value" conditions), unless a suitable low-affinity competitor is available for displacement experiments.[58] Generally, ITC can provide information on the reaction stoichiometry, but for the analysis of more complex reactions, requires independent information on the possible complex states.[59]

## CONCLUSIONS

In the present work, we have developed a new approach to extend sedimentation velocity analytical ultracentrifugation into the low picomolar concentration range and demonstrated how this can be used to determine the $K_D$ of binding between EGFP and a monoclonal IgG antibody of 20 pM. Previously, the useable concentration range of FDS-SV was considered to be 0.1 nM to 10 $\mu$M fluorescein,[20,21] and the lowest $K_D$ measurable by FDS-SV was characterized to be "10 nM or less".[20] Obviously, precise detection and $K_D$ limits will depend on the fluorophore, but we have demonstrated in the present work limits that are two or more orders of magnitude lower.

In summary, the key considerations for practical work at such low considerations in FDS-SV are (1) the careful choice of the PMT voltage and laser power (where this adjustment is possible) so as to obtain the best possible signal/noise ratio, (2) the choice of a carrier protein (other than BSA) that can be shown in control experiments to not contribute to the signal itself, to be inert with respect to the protein(s) of interest, and to effectively block surface adsorption of the protein of interest, (3) the data acquisition over a long time interval well past the sedimentation of the proteins of interest, (4) for the $c$(s) analysis, the graphical determination of the meniscus from the Raman offset visible at the air/water interface, and (5) the inclusion of as many scans as possible.

This work adds a unique tool to the analysis of high-affinity interactions. We believe the most important opportunity of FDS-SV is the observation, in free solution, of not only the degree of binding of a fluorescent ligand but, simultaneously, also the number and size of complexes and their ligand binding. This will offer the potential to study multistep and multicomponent interactions, possibly integrated with other biophysical methods in global multimethod analyses.[47] Importantly, FDS-SV inherits from SV with conventional optical detection the compatibility with detergent and nanodisc systems for the study of solubilized or reconstituted membrane proteins.[60,61]

## ASSOCIATED CONTENT

### Supporting Information

Method S1: simulation of kinetically limited binding. Theory S1: lower bounds for apparent $K_D$ estimates from kinetically limited binding. Figure S1: signal increase at the air/water meniscus from Raman scattering for $H_2O$, $H_2O$/EtOH, and $D_2O$. Figure S2: sedimentation coefficient distributions observed by FDS-SV for (unlabeled) BSA at different concentrations, in the presence and absence of EGFP. Figures S3 and S4: simulated kinetically limited binding data and best-fit impostor equilibrium isotherms as a function of chemical on-rate constant and reaction time. Figures S5 and S6: simulated kinetically limited mixing and predilution experiments as a function of chemical on-rate constant. Figure S7: fit of the SPR data with a model for a distribution of sites with different affinity and kinetic rate constants. This material is available free of charge via the Internet at http://pubs.acs.org.

## AUTHOR INFORMATION

### Corresponding Author

*E-mail: Peter.Schuck@nih.gov. Tel: 301 4351950.

### Notes

The authors declare no competing financial interest.

## ACKNOWLEDGMENTS

We thank Dr. George H. Patterson for a supply of EGFP and for helpful discussions. This work was supported by the Intramural Research Programs of the National Institute of Biomedical Imaging and Bioengineering and the National Institute of Child Health and Human Development, National Institutes of Health.

## REFERENCES

(1) Wolberger, C. *Annu. Rev. Biophys. Biomol. Struct.* **1999**, *28*, 29−56.

(2) Gavin, A. C.; Bösche, M.; Krause, R.; Grandi, P.; Marzioch, M.; Bauer, A.; Schultz, J.; Rick, J. M.; Michon, A. M.; Cruciat, C. M.; Remor, M.; Höfert, C.; Schelder, M.; Brajenovic, M.; Ruffner, H.; Merino, A.; Klein, K.; Hudak, M.; Dickson, D.; Rudi, T.; Gnau, V.;

Bauch, A.; Bastuck, S.; Huhse, B.; Leutwein, C.; Heurtier, M.; Copley, R. R.; Edelmann, A.; Querfurth, E.; Rybin, V.; Drewes, G.; Raida, M.; Bouwmeester, T.; Bork, P.; Seraphin, B.; Kuster, B.; Neubauer, G.; Superti-furga, G.; Bo, M.; Ho, C. *Nature* **2002**, *415*, 141−147.
(3) Mayer, M. L. *Curr. Opin. Neurobiol.* **2011**, *21*, 283−290.
(4) Ferré, S.; Ciruela, F.; Woods, A. S.; Lluis, C.; Franco, R. *Trends Neurosci.* **2007**, *30*, 440−446.
(5) Hey, T.; Fiedler, E.; Rudolph, R.; Fiedler, M. *Trends Biotechnol.* **2005**, *23*, 514−522.
(6) Caravella, J.; Lugovskoy, A. *Curr. Opin. Chem. Biol.* **2010**, *14*, 520−528.
(7) Torchilin, V. P. *Eur. J. Pharm. Sci.* **2000**, *11*, S81−S91.
(8) Blech, M.; Peter, D.; Fischer, P.; Bauer, M. M. T.; Hafner, M.; Zeeb, M.; Nar, H. *J. Mol. Biol.* **2013**, *425*, 94−111.
(9) Friguet, B.; Chaffotte, A. F.; Djavadi-Ohaniance, L.; Goldberg, M. E. *J. Immunol. Methods* **1985**, *77*, 305−319.
(10) Fried, M.; Crothers, D. M. *Nucleic Acids Res.* **1981**, *9*, 6505−6525.
(11) Foulds, G. J.; Etzkorn, F. A. *Nucleic Acids Res.* **1998**, *26*, 4304−4305.
(12) Senear, D. F.; Brenowitz, M. *J. Biol. Chem.* **1991**, *266*, 13661−13671.
(13) Gauglitz, G.; Proll, G. *Adv. Biochem. Eng. Biotechnol.* **2007**, *109*, 395−432.
(14) Schuck, P. *Annu. Rev. Biophys. Biomol. Struct.* **1997**, *26*, 541−566.
(15) MacGregor, I. K. K.; Anderson, A. L. L.; Laue, T. M. *Biophys. Chem.* **2004**, *108*, 165−185.
(16) Svedberg, T.; Rinde, H. *J. Am. Chem. Soc.* **1924**, *46*, 2677−2693.
(17) Lebowitz, J.; Lewis, M. S.; Schuck, P. *Protein Sci.* **2002**, *11*, 2067−2079.
(18) Howlett, G. J.; Minton, A. P.; Rivas, G. *Curr. Opin. Chem. Biol.* **2006**, *10*, 430−436.
(19) Harding, S. E.; Rowe, A. J. *Biochem. Soc. Trans.* **2010**, *38*, 901−907.
(20) Kroe, R. R.; Laue, T. M. *Anal. Biochem.* **2009**, *390*, 1−13.
(21) Kingsbury, J. S.; Laue, T. M. *Methods Enzym.* **2011**, *492*, 283−304.
(22) Zhao, H.; Berger, A. J.; Brown, P. H.; Kumar, J.; Balbo, A.; May, C. A.; Casillas, E.; Laue, T. M.; Patterson, G. H.; Mayer, M. L.; Schuck, P. *J. Gen. Physiol.* **2012**, *139*, 371−388.
(23) Zhao, H.; Casillas, E.; Shroff, H.; Patterson, G. H.; Schuck, P. *PLoS One* **2013**, *8*, e77245.
(24) Zhao, H.; Ghirlando, R.; Piszczek, G.; Curth, U.; Brautigam, C. A.; Schuck, P. *Anal. Biochem.* **2013**, *437*, 104−108.
(25) Ghirlando, R.; Balbo, A.; Piszczek, G.; Brown, P. H.; Lewis, M. S.; Brautigam, C. A.; Schuck, P.; Zhao, H. *Anal. Biochem.* **2013**, *440*, 81−95.
(26) Zhao, H.; Lomash, S.; Glasser, C.; Mayer, M. L.; Schuck, P. *PLoS One* **2013**, *8*, e83439.
(27) Lyons, D. F.; Lary, J. W.; Husain, B.; Correia, J. J.; Cole, J. L. *Anal. Biochem.* **2013**, *437*, 133−137.
(28) Zhao, H.; Berger, A. J.; Brown, P. H.; Kumar, J.; Balbo, A.; May, C. A.; Casillas, E.; Laue, T. M.; Patterson, G. H.; Mayer, M. L.; Schuck, P. *J. Gen. Physiol.* **2013**, *141*, 747−749.
(29) Patterson, G. H.; Knobel, S. M.; Sharif, W. D.; Kain, S. R.; Piston, D. W. *Biophys. J.* **1997**, *73*, 2782−2790.
(30) Schuck, P. *Biophys. J.* **2000**, *78*, 1606−1619.
(31) Zhao, H.; Brautigam, C. A.; Ghirlando, R.; Schuck, P. *Current Protocols in Protein Science* **2013**, DOI: 10.1002/0471140864.ps2012s71.
(32) Narayan, R.; Nityananda, R. *Ann. Rev. Astron. Astrophys.* **1986**, *24*, 127−170.
(33) Brown, P. H.; Balbo, A.; Schuck, P. *Biomacromolecules* **2007**, *8*, 2011−2024.
(34) Bailey, M. F.; Angley, L. M.; Perugini, M. A. *Anal. Biochem.* **2009**, *390*, 218−220.
(35) Burikov, S.; Dolenko, T.; Patsaeva, S.; Starokurov, Y.; Yuzhakov, V. *Mol. Phys.* **2010**, *108*, 2427−2436.
(36) Wood, R. *Phys. Rev.* **1934**, *45*, 392−394.
(37) Mok, Y.-F.; Ryan, T. M.; Yang, S.; Hatters, D. M.; Howlett, G. J.; Griffin, M. D. W. *Methods* **2011**, *54*, 67−75.
(38) Van Dieck, J.; Fernandez-Fernandez, M. R.; Veprintsev, D. B.; Fersht, A. R. *J. Biol. Chem.* **2009**, *284*, 13804−13811.
(39) Luta, G.; Ionescu, M. S. *Rom. J. Biophys.* **2002**, *12*, 91−96.
(40) Kumagai, A.; Ando, R.; Miyatake, H.; Greimel, P.; Kobayashi, T.; Hirabayashi, Y.; Shimogori, T.; Miyawaki, A. *Cell* **2013**, *153*, 1602−1611.
(41) Davies, D. R.; Chacko, S. *Acc. Chem. Res.* **1993**, *26*, 421−427.
(42) Schuck, P. *Anal. Biochem.* **2003**, *320*, 104−124.
(43) Stafford, W. F. *Methods Enzym.* **2000**, *323*, 302−325.
(44) Schuck, P. *Biophys. J.* **2010**, *98*, 2005−2013.
(45) Foote, J.; Milstein, C. *Nature* **1991**, *352*, 530−532.
(46) Svitel, J.; Boukari, H.; Van Ryk, D.; Willson, R. C.; Schuck, P. *Biophys. J.* **2007**, *92*, 1742−1758.
(47) Zhao, H.; Schuck, P. *Anal. Chem.* **2012**, *84*, 9513−9519.
(48) Schuck, P.; Millar, D. B.; Kortt, A. A. *Anal. Biochem.* **1998**, *265*, 79−91.
(49) Day, E. S.; Capili, A. D.; Borysenko, C. W.; Zafari, M.; Whitty, A. *Anal. Biochem.* **2013**, *440*, 96−107.
(50) Melikishvili, M.; Rodgers, D. W.; Fried, M. G. *DNA Repair* **2011**, *10*, 1193−1202.
(51) Rispens, T.; Ooijevaar-de Heer, P.; Derksen, N. I. L.; Wolbink, G.; van Schouwenburg, P. a; Kruithof, S.; Aalberse, R. C. *Anal. Biochem.* **2013**, *437*, 118−122.
(52) Dam, J.; Schuck, P. *Biophys. J.* **2005**, *89*, 651−666.
(53) Hwang, L. C.; Wohland, T. *Cell Biochem. Biophys.* **2007**, *49*, 1−13.
(54) Swift, J. L.; Heuff, R.; Cramb, D. T. *Biophys. J.* **2006**, *90*, 1396−1410.
(55) Owen, B.; McMurray, C. *Protocol Exchange* **2009**, DOI: 10.1038/nprot.2009.80.
(56) Bacia, K.; Schwille, P. *Nat. Protoc.* **2007**, *2*, 2842−2856.
(57) Carriba, P.; Navarro, G.; Ciruela, F.; Ferré, S.; Casadó, V.; Agnati, L.; Cortés, A.; Mallol, J.; Fuxe, K.; Canela, E. I.; Lluís, C.; Franco, R. *Nat. Methods* **2008**, *5*, 727−733.
(58) Velazquez Campoy, A.; Freire, E. *Nat. Protoc.* **2006**, *1*, 186−191.
(59) Houtman, J. C.; Brown, P. H.; Bowden, B.; Yamaguchi, H.; Appella, E.; Samelson, L. E.; Schuck, P. *Protein Sci.* **2007**, *16*, 30−42.
(60) Ebel, C. *Methods* **2011**, *54*, 56−66.
(61) Inagaki, S.; Ghirlando, R.; Grisshammer, R. *Methods* **2013**, *59*, 287−300.